Journal of The Electrochemical Society, **157** (8) B1103-B1108 (2010)
0013-4651/2010/157(8)/B1103/6/$28.00 © The Electrochemical Society

Intermediate-Temperature, Proton-Conducting Membranes of Hafnium Phosphate and Zirconium Phosphate/Borate/Sulfate

Yuanzhi Li,[a,b] Emi Muto,[a] Yoshitaka Aoki,[a,c] and Toyoki Kunitake[a,d,z]

[a]*Frontier Research System, Institute of Physical and Chemical Research, Hirosawa, Wako 351-0104, Japan*
[b]*Key Laboratory of Silicate Materials Science and Engineering, Wuhan University of Technology, Ministry of Education, Wuhan 430070, People's Republic of China*

Uniform, defect-free nanofilms (around 100 nm thick) of hafnium phosphate were prepared via layer-by-layer deposition of precursor solution of metal alkoxides and were shown to give practically useful proton conductivity at 300–400°C as fuel cell electrolyte membrane. Annealing of the deposited precursor film at 500°C gave a lower area specific resistance (R_{AS}) than that at 400°C, and this effect was coincident with the formation of the pyrophosphate unit. The best (lowest) R_{AS} value of less than 0.1 Ω cm^2 for hafnium phosphate membrane (annealing at 500°C, 291 nm thick, conductivity of 3×10^{-4} S cm^{-1} at 320°C) was comparable to that of a nanofilm of an yttrium-doped zirconium phosphate. The R_{AS} values of nanofilms of zirconium sulfate and zirconium borate were 2–3 orders higher than that of the corresponding zirconium phosphate. It is clear from these results that nanofilms of various solid acids are promising candidates for the electrolyte membrane of fuel cells operating at the intermediate temperatures of 300–400°C.
 [DOI: 10.1149/1.3432600]

Manuscript submitted February 8, 2010; revised manuscript received April 27, 2010. Published June 3, 2010.

Solid acid catalysis has been widely used within the petrochemical industry and is attracting increasing attention due to its environment-friendly feature.[1] Solid acid catalysts are composed of wide-ranging acidic materials including clay minerals, zeolites, metal oxides and sulfides, metal hydroxides, and heteropoly acids. The acid sites may either be Broensted or Lewis type. Being a most popular class of solid acids, zeolites are microporous crystalline solids of aluminosilicate with well-defined cage structures of SiO_2 and Al_2O_3 units. Such basic atomic connectivity must be maintained in the aluminosilicate compounds regardless if they are crystalline or not.

The development of electrolyte membranes that are composed of inexpensive materials and are operable at the intermediate temperatures of 200–400°C is strongly desired to enable the next-generation fuel cell (FC) technology. The novel electrolyte membrane should show satisfactory material stability, effective proton conduction, efficient redox reaction and the consequent reduction of electrocatalyst loading, improvement in CO tolerance, and manageable heat recovery.[2] In addition, anhydrous proton conduction in the intermediate-temperature regime eliminates the elaborate water management required for Nafion-based polymer electrolyte fuel cells (PEFCs).

The idea of using inorganic solid acid as FC electrolyte membrane was examined in our previous study.[3] Surprisingly, amorphous nanofilms of aluminosilicate in fact contained acid sites that enabled efficient proton conduction across the film. A 70 nm thick amorphous aluminosilicate film gave practically useful proton conductivity at 300–400°C as an electrolyte membrane of an FC. This was a strong indication that the local atomic connection of the zeolite structure that provides acid sites was basically preserved even in the ultrathin amorphous film. Our subsequent study[4] demonstrated that many of the silica-based double oxides gave rise to proton conductivity of different degrees in the form of amorphous nanofilms.

The presence of effective acid sites was also shown in phosphate materials.[5] Amorphous nanofilms of zirconium phosphate exhibited a practically useful level of proton conductivity at 300°C. A covalent network of metal and phosphate species provided quite robust nanofilms whose morphology and proton conductivity remained unchanged for hundreds of hours during the electrochemical examination of up to 400°C. These findings suggest an exciting possibility of developing a rich variety of proton-conducting nanofilms, even more so than the case of silica-based double oxides. Uniform amorphous nanofilms may be obtainable from a large combination of metal species and multivalent oxyacids. Therefore, they provide a valuable opportunity to conduct an extensive search for materials that would give superior proton conductivity and robustness. An advantage of the amorphous texture is that the variety of combination is not restricted by the stoichiometry of the two major components. Certain metal phosphates[6] and borates[7] exhibit highly efficient proton conductivities as crystalline compounds. Unfortunately, these compounds, as such, did not produce robust uniform nanofilms probably due to their crystalline nature. Because the basic atomic framework is common, their amorphous counterparts may provide acid sites for proton conduction, if properly prepared.

As the first step of materials search, we replaced the zirconium species with hafnium, in the current study, as the two metal species belong to the identical IV family in the periodic table. We assumed that they would form closely related covalent networks. The film formation and proton conductivity of hafnium phosphate were compared with those of zirconium phosphate. As for the multivalent oxyacid, we chose boric acid and sulfuric acid by considering the chemical stability of their metal oxygen bonds, and the electrochemical behavior of their zirconium compounds were compared with those of the previously reported results of zirconium phosphate. Nanofilms of zirconium sulfate and zirconium borate were prepared to examine their proton conductivities in relation to their phosphate counterpart.

Experimental

Materials.— 2-Methoxyethanol (reagent grade), ethanol (reagent grade), diphosphorous pentoxide, boric acid, ethylenediamine, and anhydrous zirconium tetra-*n*-butoxide (85–90%) were obtained from Kanto Chemical. Hafnium tetra-*n*-butoxide (95%) and yttrium methoxyethoxide (15–18% in methoxyethanol) were obtained from Gelest Inc. Yttrium tetra-*n*-butoxide and indium tin oxide (ITO) coated glass substrate (30 nm thick ITO layer, 70 Ω) were obtained from Aldrich. Sulfuric acid was bought from Junsei Chemical.

Preparation of thin films of metal phosphate/borate/sulfate.— The ITO substrate (2.5 × 4 cm) was cleaned by sonication in ethanol for 2 min and then dried by flushing nitrogen gas. A thin film of amorphous hafnium phosphate was deposited in a layer-by-layer fashion by the surface sol–gel process. The precursor sol was prepared as follows: 0.496 g of hafnium tetra-*n*-butoxide was added to 20 mL of 2-methoxyethanol. The mixture was vigorously stirred for 5 min at room temperature. P_2O_5 (0.213 g) was added to 30 mL of 2-methoxyethanol and the mixture was sonicated in an

[c] Present address: Graduate School of Engineering, Hokkaido University, Sapporo 060-8628, Japan.
[d] Present address: FAIS, Kitakyushu 808-0135, Japan and NanoMembrane Technologies, Wako-Riken, Saitama 351-0104, Japan.
[z] E-mail: kunitake@ruby.ocn.ne.jp

ultrasonic bath for 6 min until a transparent solution was obtained. The two solutions were mixed and vigorously stirred for 10 min at room temperature. The final solution was prepared by mixing 9 mL of the Hf/P_2O_5 solution and 1 mL of water. The final concentration of the total metal atoms in the precursor solution was 18 mmol/L.

Hafnium phosphate layer was deposited onto the ITO substrate by spin coating with a Mikasa 1H-D7 spin coater. An ITO glass slide (2.5×4 cm) was placed on the rotating stage of a spin coater. 250 μL of the precursor sol was dropped onto the ITO slide, and spin coating was started at a rotating rate of 3000 rpm for 20 s. The deposited gel layer was dried by hot air from an electric hair dryer for 2 min. This cycle of sol–gel process, spin coating, and drying was repeated 15 times. The gel film thus obtained was annealed at 400°C for 1 h. The cycle of multiple depositions and annealing was repeated two times.

Precursor solutions of zirconium (yttrium) borate and zirconium (yttrium) sulfate were similarly prepared by employing solutions of H_3BO_4 in 2-methoxyethanol and H_2SO_4–ethylenediamine salt in 2-methoxyethanol, respectively, in place of P_2O_5 in 2-methoxyethanol. 3 mol of boric acid was used against 1 mol of the total metal species, but only 0.1 mol of sulfuric acid was used against 1 mol of the total metal species because of the solubility problem. Film deposition was conducted in the same way by using appropriate numbers of the deposition cycle so that proper film thickness was attained.

Characterization.— Reflectance Fourier transform infrared (FTIR) spectra were taken on a ThermoNicolet Nexus670 spectrometer. Silicon wafer coated with Pt film was used as the reflectance standard as well as substrate for the film. Thin films of hafnium phosphate were prepared on a silicon wafer coated with Pt film by the same procedure as mentioned above. X-ray diffraction patterns were obtained on a Rigaku DMAX X-ray diffractometer using Cu Kα radiation. The elemental composition of the film was determined by an X-ray photoelectron spectroscope (XPS, VG Science, ESCALAB250). The film morphology was observed by a scanning electron microscope (SEM, Hitachi S-5200). The details of these procedures have been described in our previous paper.[4]

Impedance spectroscopy.— The proton conductivity of the as-fabricated films was measured by the ac impedance method. Pt electrodes (100 nm thick, 1 mm in diameter) were deposited on the top of the nanofilm through a shadow mask to form a Pt/film/ITO stack. The electrical lead of Au fine wire (0.05 mmϕ) was attached to the Pt and ITO electrodes by using Pt paste (Nilaco). Impedance spectroscopy was carried out for the stack by a frequency analyzer (Solartron 1250) in a frequency range of $10–10^7$ Hz at an ac amplitude of 20 mV. The temperature of a specimen was adjusted by the electrical furnace. All the measurements were carried out under the flow of dry air or under humid air as saturated with water at 18°C.

Results and Discussion

Fabrication and characterization of hafnium phosphate films.— Thin films of hafnium phosphate were deposited on ITO substrate in a layer-by-layer fashion by using mixed solutions of hafnium tetra-*n*-butoxide and P_2O_5 as starting materials. The atomic ratio in the precursor mixture is Hf/P = 1.0/3.0, and the resulting films as annealed at 400, 450, and 500°C are denoted as HfP_3-400, HfP_3-450, and HfP_3-500, respectively. However, the atomic ratio, Hf/P/O, of the HfP_3-500 nanofilm as measured by XPS is 1/3.3/10.7. The observed Hf/P ratio is smaller than that in the precursor solution. This difference may be caused by some loss of hafnium tetra-*n*-butoxide during the spin coating process. The FTIR result shows the existence of proton in the HfP_3-500 nanofilm. By applying the charge balance by proton to the XPS composition data, the elemental composition of the hafnium phosphate nanofilm, HfP_3-500, was estimated to be $Hf_{1.0}H_{0.9}P_{3.3}O_{10.7}$.

Figure 1 gives the reflectance FTIR spectra of these films. In the HfP_3-400 film, two shoulder peaks appear at 972 and 1099 cm^{-1} in

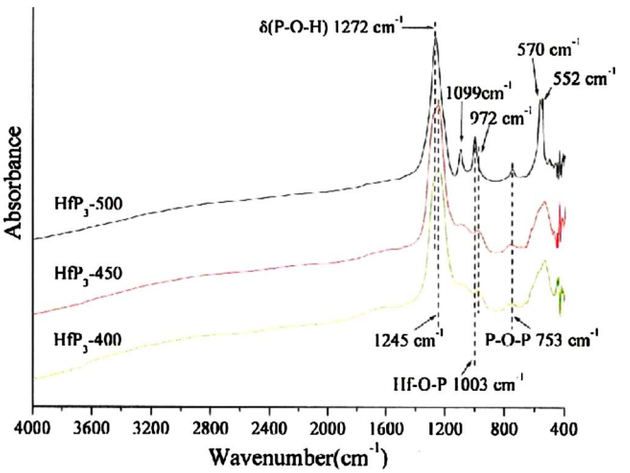

Figure 1. (Color online) Reflectance FTIR spectra of nanofilms of hafnium phosphate as annealed at different temperatures.

the P–O stretching region and are assigned to Hf–O–P and to HO–P vibrations. A small band appearing at 753 cm^{-1} is attributed to P–O–P vibration,[8] indicating the presence of the pyrophosphate moiety. A strong sharp peak was observed at 1245 cm^{-1} with a shoulder peak at 1272 cm^{-1}, which are assigned to different deformation modes of δ(POH),[9] which arise from the coexistence of two types of the POH group. The O–H stretching mode above 3000 cm^{-1} is represented by a very broad band probably due to extensive hydrogen bonding. The FTIR spectrum does not give detectable changes when the annealing temperature is raised from 400 to 450°C. However, the annealing at 500°C leads to the appearance of two sharp peaks at 1099 and 1003 cm^{-1} (Hf–O–P and HO–P vibrations) and a blueshift from 1003 to 972 cm^{-1}. The 1245 cm^{-1} peak is shifted to a sharper peak at 1272 cm^{-1}. These observations suggest that the pyrophosphate unit becomes predominant upon annealing at 500°C.

In our related study on yttrium-doped zirconium phosphate,[5] we showed that the pyrophosphate unit was formed only after calcination at 400°C, while the monophosphate unit mainly existed by annealing at 120°C. We are now assured that annealing at higher temperature promotes formation of the pyrophosphate structure in both of the zirconium and hafnium systems. These structural changes commonly give rise to more efficient proton conduction, as discussed below. Apparently, the basic structural feature of the phosphate moiety must be similar between the Zr and Hf thin films.

In X-ray diffraction experiments, significant peaks are not detected for the HfP_3-400 and HfP_3-450 nanofilms, while the HfP_3-500 nanofilm has three weak peaks at 18.7, 21.6, and 36.3°. These peaks are consistent with the diffraction of the (111), (200), and (311) planes of cubic hafnium pyrophosphate (HfP_2O_7, JCPDS 37-1494), respectively. Apparently, the nanofilms annealed up to 450°C are basically amorphous, but annealing at 500°C produces a certain crystalline fraction of cubic hafnium pyrophosphate.

Figure 2 presents electron microscopic observation of nanofilms of HfP_3-400 and HfP_3-500. The top-view SEM image of Fig. 2a indicates that the surface of the HfP_3-400 nanofilm is uniform without pinholes, cracks, or aggregated particles. The cross-sectional SEM image of Fig. 2b demonstrates that the film has a uniform thickness of 273 nm. Because we repeated 45 cycles of the layer-by-layer process, the individual cycle of sol–gel deposition led to the formation of a 6.1 nm thick layer. Similar morphological characteristics of uniform surface and constant thickness are observed for the HfP_3-500 film (Fig. 2c and d). The thickness, however, de-

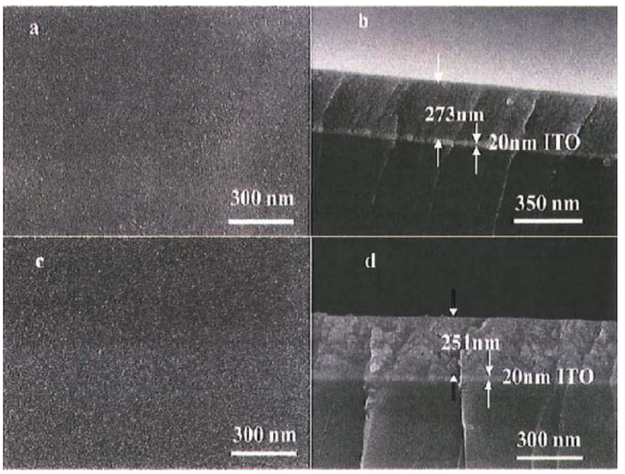

Figure 2. (Color online) SEM images of the nanofilms. HfP_3-400 nanofilm (a) top view and (b) cross section and HfP_3-500 nanofilm (c) top view and (d) cross section.

creases from 273 to 251 nm (8% shrinkage, compare Fig. 2b and d) by raising the annealing temperature. The denser film is a better proton conductor (see below).

Fabrication of zirconium (yttrium) phosphate/borate/sulfate nanofilms.— Uniform, defect-free nanofilms have been available from zirconium phosphate and yttrium-doped zirconium phosphate, and the zirconium moiety can be replaced with hafnium, as we discussed above. It is also desirable to see if the phosphate moiety is replaceable with other multivalent acid moieties such as borate and sulfate. Essentially identical fabrication procedures were used for the fabrication of nanofilms of zirconium borate and zirconium sulfate.

Three kinds of nanofilms were prepared for zirconium borate with and without yttrium doping at an annealing temperature of 400°C: ZrB_3-400, $Zr_{0.95}Y_{0.05}B_3$-400, and $Zr_{0.9}Y_{0.1}B_3$-400. In all cases, uniform, defect-free films were obtainable. Figure 3 displays SEM observation of zirconium borate nanofilms. Without regard to yttrium doping, they all show cross sections of constant thickness and uniform (without structure) surfaces. The film thickness is 80 nm in all cases. Crystalline morphologies are not found. Borate moiety can clearly replace the phosphate moiety to form uniform, amorphous nanofilms. Similar results are obtainable when 10 mol % of sulfate is used in place of phosphate (data not shown) at an annealing temperature of 400°C: $ZrS_{0.1}$-400, $Zr_{0.95}Y_{0.05}S_{0.1}$-400, and $Zr_{0.9}Y_{0.1}S_{0.1}$-400.

The atomic ratio as measured by XPS is 0.96/0.04/0.49 for $Zr_{0.95}Y_{0.05}B_3$-400 and 0.95/0.05/1.03 for $Zr_{0.95}Y_{0.05}S_{0.1}$-400. The atomic ratio of the Zr and Y metals in the nanofilm is essentially identical to those of the respective feeds, but the boron ratio is much

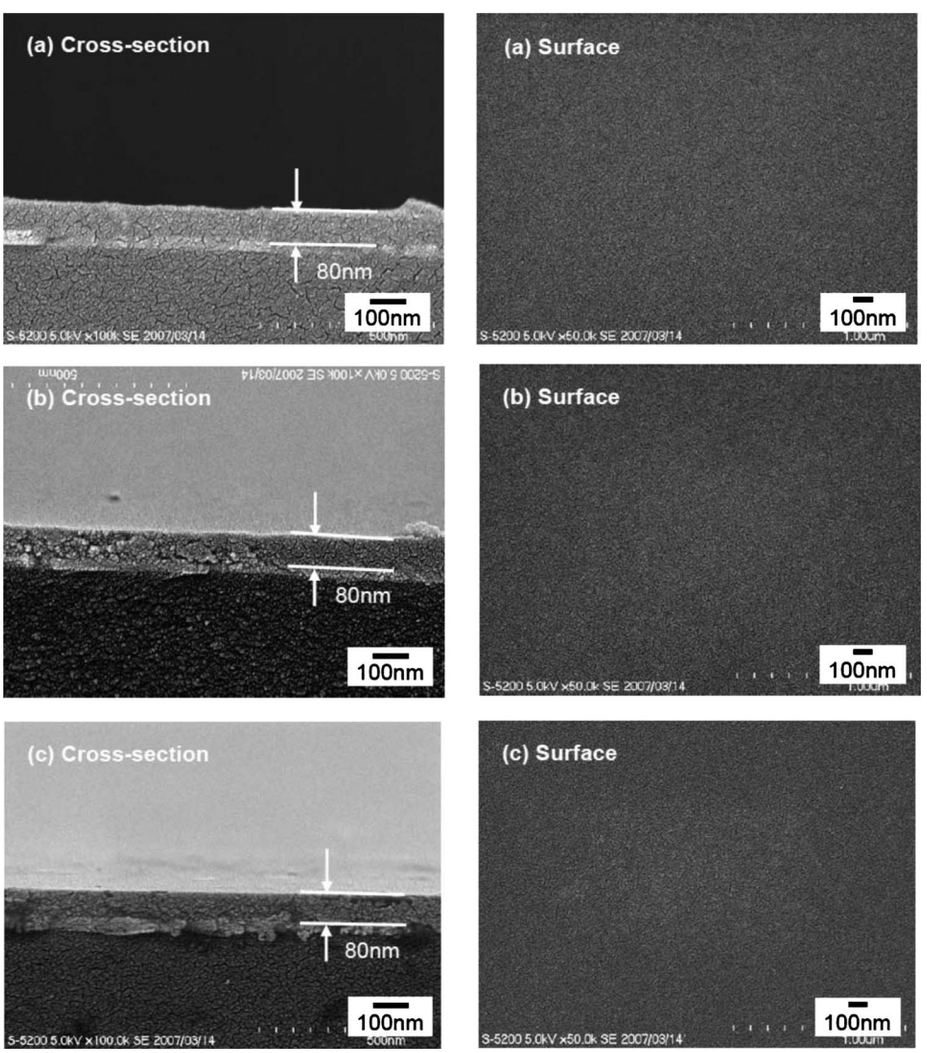

Figure 3. SEM images (cross section and top view) of nanofilms of (a) ZrB_3-400, (b) $Zr_{0.95}Y_{0.05}B_3$-400, and (c) $Zr_{0.9}Y_{0.1}B_3$-400.

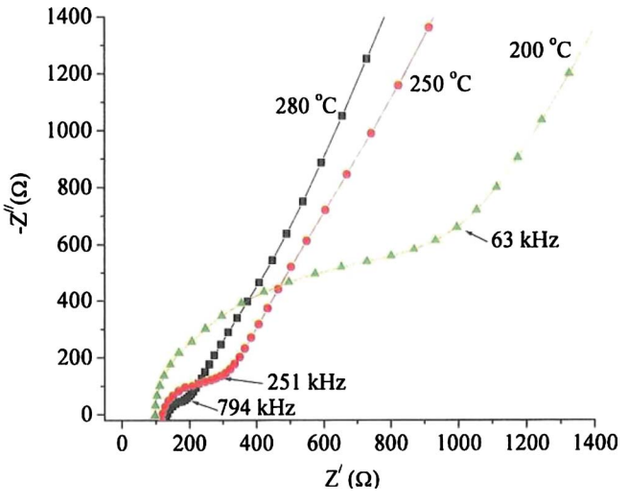

Figure 4. (Color online) Impedance responses of the hafnium phosphate nanofilm, HfP_3-500, under dry air.

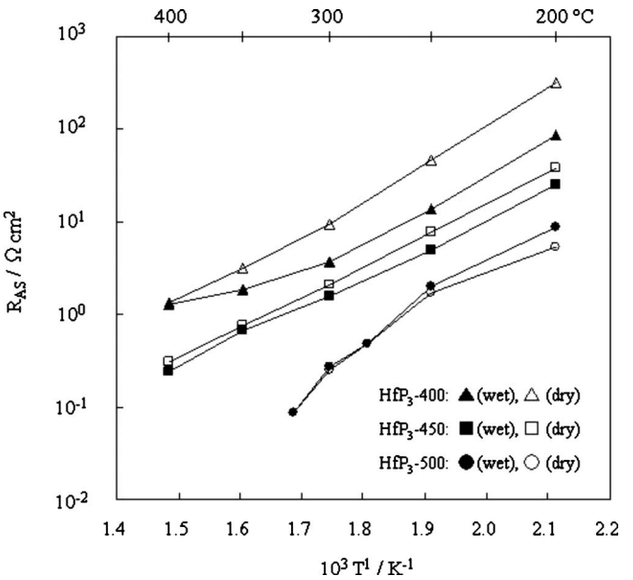

Figure 5. Temperature dependence of area-specific resistance (R_{AS}) of hafnium phosphate nanofilms, as annealed at 400, 450, and 500°C, under wet and dry conditions.

smaller in the film than in the feed, and the sulfur ratio is much larger in the film than in the feed. The metal/acid ratio in these cases may be optimized during the spin coating (that is, film formation) process in such a way that properly stable covalent networks are formed. In the borate film, the atomic ratio of metal and borate components is 2:1 and this ratio suggests that the borate unit is connected to two zirconia moieties. Unfortunately, the nature of the network structure cannot be determined from the available data. However, the metal/sulfate ratio is 1:1 for the zirconium sulfate film. A given zirconia center is, on average, connected to two sulfate units and two neighboring zirconia units. Several different network structures are conceivable in this case as well.

These results are quite in contrast to that of the phosphate system, where the metal/acid ratio was always close to that of the respective feed and 3 mol of the phosphate unit were readily incorporated against 1 mol of the metal moiety. The monophosphate unit can form a stable covalent linkage among themselves, as exemplified by pyrophosphate and adenosine triphosphate. In contrast, covalent linking between acid units is not stable in borate and sulfate. Therefore, excess (nonstoichiometric) feeds of the phosphate moiety may be readily incorporated into the film without loss, whereas the content of the borate and sulfate units is apparently limited by simple stoichiometry

Proton conduction of hafnium phosphate nanofilm.— Figure 4 gives typical cases of impedance response of the hafnium phosphate nanofilm at different temperatures under the flow of dry air. Impedance spectra were collected as real (Z') and imaginary (Z'') components of the complex impedance. All the spectra consist of a single semicircle in the high frequency region and near the vertical "spike" in the low frequency region. The high frequency semicircle is attributed to the impedance response of proton conduction in bulk film. It becomes smaller monotonously with increasing temperature. Additional semicircles that could be related to the conduction through grain boundary or impurity layer do not appear at any temperature. The low frequency spike corresponds to the charge buildup at the interface of film/electrode, indicating that no charge transfer occurs across the film and electron-conductive electrode.

The impedance spectra were analyzed to calculate ion conductivity by the nonlinear least-squares fitting with an equivalent circuit model. The area specific resistance (R_{AS}) was determined from across-the-film resistance. The details of measurement and analysis of impedance spectra were described elsewhere.[10] Figure 5 shows the temperature dependence of R_{AS} for three hafnium phosphate nanofilms that are annealed at different temperatures. The R_{AS} value for the HfP_3-400 film decreases from 320 to 1.4 Ω cm^2 under the flow of dry air, as the measurement temperature is raised from 200 to 400°C. It is improved by humidity, and, at 200°C, it is 3.7 times larger under the flow of wet air (saturated with water at 18°C, water concentration of 2 vol %) than that under dry air. This conductivity difference, which probably arises from adsorbed water, decreases with rising temperature of measurement, and it disappears at 400°C. The effect of adsorbed water is displayed most strongly at the annealing temperature of 400°C (HfP_3-400 nanofilm) and becomes less apparent when the nanofilm is annealed at higher temperatures. In fact, the HfP_3-500 nanofilm shows a small R_{AS} difference of only 3.2 Ω cm^2 at 200°C.

Higher annealing temperature clearly results in lower R_{AS} values. For example, at 300°C in dry air, the R_{AS} value of the HfP_3-450 and HfP_3-500 nanofilms is 4.5 and 37 times smaller, respectively, relative to that of the HfP_3-400 nanofilm. This effect is attributed to annealing-derived structural changes involving (at least) partial conversion from phosphate to pyrophosphate, as evidenced by FTIR spectra. We recognize that the humidity effect becomes very small when the annealing temperature is highest (500°C). It is reasonable to assume that the network structure of amorphous hafnium (pyro)-phosphate is stabilized by such high temperature annealing and that humidity becomes less prone to affect the proton conductivity of the film.

The R_{AS} value of the HfP_3-500 film decreases from 5.5 Ω cm^2 at 200°C to 0.26 Ω cm^2 at 300°C under dry air. At the temperature of 320–400°C, it is smaller than an R_{AS} value of 0.15 Ω cm^2 that is considered sufficient for a practical electrolyte membrane in commercial FCs.

A crude estimation of the apparent activation energy (E_a) of proton conduction gives 0.44 eV for the HfP_3-500 film from the data of Fig. 5. E_a values are less than 0.1 eV for humidity-sensitive proton conductors, in which proton conduction is realized by charge transport via H_3O^+ or $H_5O_2^+$.[11] However, anhydrous proton conductors via proton hopping mechanism give $E_a > 0.2$ eV.[12,13] In our previous work,[5] we proposed that proton conduction in the nanofilm of amorphous Y-doped zirconium phosphate is mediated by the transport of hydrogen-bonded proton via rearrangement of intermolecular hydrogen bond, in the absence of the influence of adsorbed water. For the present nanofilm, the conductivity was similarly in-

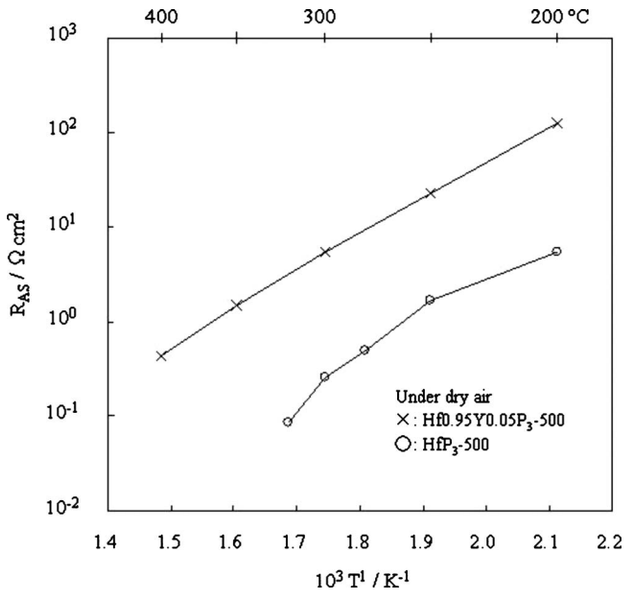

Figure 6. Temperature dependence of R_{AS} of hafnium phosphate nanofilms with and without yttrium doping. Annealed at 500°C.

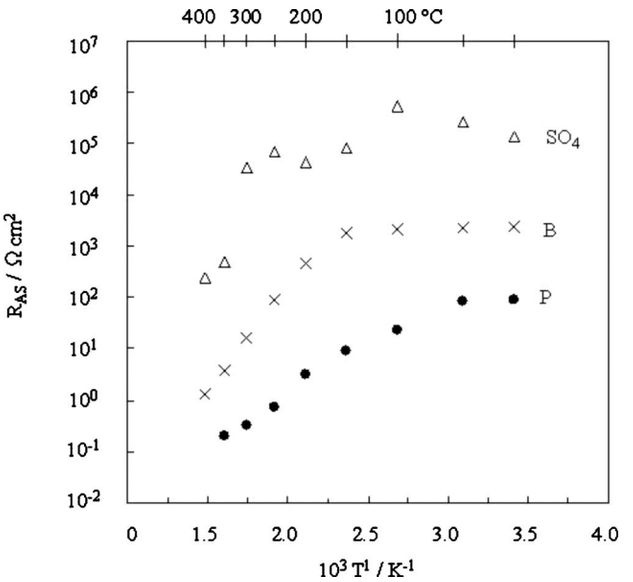

Figure 7. Temperature dependence of R_{AS} values of nanofilms of zirconium phosphate/borate/sulfate.

sensitive to adsorbed water in the intermediate-temperature range and a higher activation energy was found. Therefore, we may assume that an analogous mechanism of proton conduction operates in the film of HfP_3-500. Apparently, there is no difference in proton conduction mechanism between the zirconium and hafnium systems.

Proton conduction of yttrium-doped hafnium phosphate nanofilm.— We showed in our previous study that the proton conductivity of the zirconium phosphate nanofilm (annealed at 400°C) is enhanced by doping of 5 mol % yttrium: more than 10 times improvement at 340°C.[5] We expected that a similar improvement is found for the hafnium phosphate system. Contrary to our expectation, the $Hf_{0.95}Y_{0.05}P_3$-500 film gave R_{AS} values that are much higher than the corresponding undoped hafnium phosphate film (HfP_3-500) in the whole temperature range, as shown in Fig. 6. For example, R_{AS} of HfP_3-500 is 21 times smaller than that of the $Hf_{0.95}Y_{0.05}P_3$-500 film at 300°C. We cannot yet provide a proper explanation for such contrasting doping effects between the zirconium and hafnium systems. Partial replacement of the tetravalent hafnium center with a small amount of the trivalent yttrium center could create additional proton sites to recover charge balance. Unfortunately, this expectation was not fulfilled, unlike the case of zirconium phosphate nanofilm. The doping effect is influenced by various factors, including polarization of metal–oxygen bond, charge balance, and distribution of doped elements. More careful study is needed.

Comparison of proton conductivities of yttrium-doped zirconium phosphate/borate/sulfate nanofilms.— From the above-mentioned data, efficient proton conduction is clearly observed even when zirconium is replaced with hafnium. This suggests that effective proton migration is possible with a variety of solid acids in the form of nanofilm. In this respect, it is important to test if phosphate moiety is replaceable with other multivalent acid moieties. Figure 7 compares R_{AS} values of the $Zr_{0.95}Y_{0.05}B_3$-400 nanofilm and $Zr_{0.95}Y_{0.05}S_{0.1}$-400 nanofilm with that of $Zr_{0.95}Y_{0.05}P_3$-400 in the temperature range of 0–400°C. Yttrium-doped films were employed because a higher conductivity was obtained in the phosphate. Both of the borate and sulfate films show fairly constant R_{AS} values from 0 to 150°C, and then they rapidly decrease with rising temperature. The overall trend of temperature dependence is common among the three nanofilms. However, relative to the phosphate film, the borate film gives 10–100 times greater R_{AS} values and the sulfate film gives even greater values (3–4 orders of magnitude greater) in the whole temperature range. The advantage of the phosphate film in proton conduction over those of the borate and sulfate films is clearly shown.

Several hypotheses may be conceived for the difference. One is differences in strength and availability of the solid acid site. The strength of the acid site generated in a given nanofilm would certainly vary according to the solution acidity of phosphate, borate, and sulfate. At the same time, such acid strength must be influenced by individual structures characteristic of the solid state. The availability (population) of the acid site should be similarly affected by individual structures of the acid site. The atomic connectivity of metal moiety and acid moiety is not straightforward in amorphous films, and simple argument is difficult. These problems may be solved by directly measuring the amount and strength of the solid acid, and will be an important topic of our future study. A second conceivable reason is related to the molar ratio of metal and acid moieties in the nanofilm. On the basis of elemental composition data, phosphate moiety is freely incorporated into the nanofilm, whereas sulfate and borate moieties are introduced in the stoichiometric ratios. In the phosphate films, the formation of pyrophosphate units by thermal treatment enhanced proton conductivity. These results suggest that direct linking of two phosphate units is quite effective for improved proton migration. Such direct linking is not stable for the borate and sulfate systems. Why the pyrophosphate unit is advantageous for proton migration is not known at this stage; however, this is an important clue as to how to develop efficient proton conducting materials.

Thermal stability of HfP_3-500 nanofilm.— Metal oxide nanofilms are assumed to be thermally stable by their inorganic oxide network structures. Covalent metal phosphates should be similarly stable, and in fact, zirconium phosphate nanofilms displayed sufficient thermal stability for a period of at least 80 h in our previous study. To test its generality for the HfP_3-500 nanofilm, proton conductivity was measured by keeping the nanofilm at 300°C in the flow of wet air (air saturated with water at 18°C) for different periods of time. As shown in Fig. 8, proton conductivity remained unchanged for 58 h. The electrical breakdown/deterioration was not

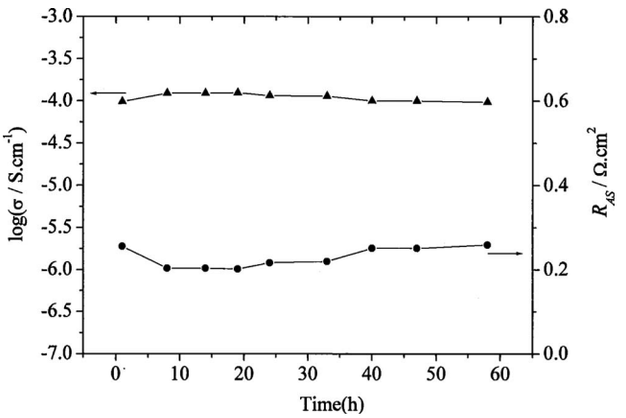

Figure 8. Time-dependent conductivity measurement of the HfP_3-500 nanofilm in the flow of wet air at 300°C.

observed during this long-time heating. The conductivity as measured again at 300°C under dry air after the heat-treatment in wet air remained unchanged.

Conclusions

It is reported that certain phosphate materials, such as SiO_2–P_2O_5,[12] P_2O_5–ZrO_2–SiO_2,[13] and TiO_2–P_2O_5,[9] reveal high proton conductivities at temperatures below 150°C under the conditions of high humidity. The presence of water incorporated in the xerogel is crucial in these cases because these materials exhibit quick deterioration of protonic conductivity due to loss of water under dry atmosphere or at elevated temperatures. Therefore, they cannot be employed as FC electrolyte membrane at intermediate temperatures of 200–400°C. In contrast, uniform, defect-free nanofilms of silica-based double oxides and zirconium phosphate, which we reported recently, are stable in this temperature region and show satisfactory proton conductivity at 300–400°C under dry conditions. In the present study as well, nanofilms of zirconium borate/sulfate are effective proton conductors, and replacement of zirconium with hafnium in the phosphate film does not suppress conductivity. We conclude from these results that practically meaningful proton conductivity at around 300°C is attainable with 100–200 nm thick nanofilms of metal phosphate, metal borate, and metal sulfate. The practical advantage of intermediate-temperature FCs relative to low temperature PEFCs and high temperature solid oxide FCs has been well documented. However, FC electrolyte membranes, which can be operated at the intermediate-temperature range of 200–400°C, have been scarce because many of the highly proton-conducting materials could not provide sufficiently durable membranes.

Our recent findings provide a new opportunity in this area. As mentioned in the introduction, electrolyte membranes that are operable at the intermediate-temperature range of 200–400°C under anhydrous condition possess unique advantages in constructing practical FCs. The efficient proton conductivity of the defect-free nanofilm of hafnium phosphate (R_{AS} = 0.086 Ω cm^2 at 320°C) satisfies the practical conductivity requirement in commercial FCs and is among the highest for the ceramic membranes in the temperature range of 200–400°C. We already demonstrated that defect-free nanofilms of amorphous Y-doped zirconium phosphate gave a similarly effective proton conductivity with an R_{AS} of as low as 0.085 Ω cm^2 at 340°C under anhydrous condition,[5] and that nanofilms of amorphous aluminosilicate also gave high proton conductivity with a quite low R_{AS} value of 0.24 Ω cm^2 at 400°C.[4] It is undoubted that solid acid materials of silicate-based double oxides of metals and metal compounds of multivalent acids give, in many cases, superior proton-conducting materials in the nanofilm form. The implication of this conclusion is not restricted to the design of novel FC electrolyte membranes because electrochemical hydrogen generation and various sensing devices require proton-conducting elements as key components.

Institute of Physical and Chemical Research assisted in meeting the publication costs of this article.

References

1. K. Wilson and J. H. Clark, *Pure Appl. Chem.*, **72**, 1313 (2000).
2. E. Chalkova, M. V. Fedkin, S. Komarneni, and S. N. Lvov, *J. Electrochem. Soc.*, **154**, B288 (2007).
3. Y. Aoki, E. Muto, and T. Kunitake, *Chem. Commun. (Cambridge)*, **2007**, 2396.
4. Y. Aoki, E. Muto, A. Nakao, and T. Kunitake, *Adv. Mater.*, **20**, 4387 (2008).
5. Y. Li, T. Kunitake, Y. Aoki, and E. Muto, *Adv. Mater.*, **9999**, 1 (2008).
6. M. Nagao, A. Takeuchi, P. Heo, T. Hibino, M. Sano, and A. Tomita, *Electrochem. Solid-State Lett.*, **9**, A105 (2006); P. Heo, M. Nagao, T. Kamiya, M. Sano, A. Tomita, and T. Hibino, *J. Electrochem. Soc.*, **154**, B63 (2007).
7. S. Noirault, S. Celerier, O. Joubert, M. T. Caldes, and Y. Piffard, *Adv. Mater.*, **19**, 867 (2007).
8. T. Takei, Y. Kobayashi, H. Hata, Y. Yonesaki, N. Kumada, N. Kinomura, and T. E. Mallouk, *J. Am. Chem. Soc.*, **128**, 16634 (2006).
9. M. P. Kapoor, S. Inagaki, and H. Yoshida, *J. Phys. Chem. B*, **109**, 9231 (2005).
10. H. Li and T. Kunitake, *Chem. Lett.*, **35**, 640 (2006).
11. M. Yamada, D. L. Li, I. Honma, and H. Zhou, *J. Am. Chem. Soc.*, **127**, 13092 (2005).
12. M. Yamada and I. Honma, *Angew. Chem., Int. Ed.*, **43**, 3688 (2004).
13. K. D. Kreuer, *Chem. Mater.*, **8**, 610 (1996).